Send Orders for Reprints to reprints@benthamscience.ae

Discovery of MINC1, a GTPase-Activating Protein Small Molecule Inhibitor, Targeting MgcRacGAP

Arjan J. van Adrichem[1], Annika Fagerholm[2], Laura Turunen[1], Anna Lehto[1], Jani Saarela[1], Ari Koskinen[2], Gretchen A. Repasky[1] and Krister Wennerberg[*,1,3]

[1]*Institute for Molecular Medicine Finland, University of Helsinki, Helsinki, Finland*

[2]*Laboratory of Organic Chemistry, Department of Chemistry, School of Chemical Technology, Aalto University, Espoo, Finland*

[3]*Drug Discovery Division, Southern Research Institute, Birmingham, AL, USA*

Abstract: The Rho family of Ras superfamily small GTPases regulates a broad range of biological processes such as migration, differentiation, cell growth and cell survival. Therefore, the availability of small molecule modulators as tool compounds could greatly enhance research on these proteins and their biological function. To this end, we designed a biochemical, high throughput screening assay with complementary follow-up assays to identify small molecule compounds inhibiting MgcRacGAP, a Rho family GTPase activating protein involved in cytokinesis and transcriptionally upregulated in many cancers. We first performed an in-house screen of 20,480 compounds, and later we tested the assay against 342,046 compounds from the NIH Molecular Libraries Small Molecule Repository. Primary screening hit rates were about 1% with the majority of those affecting the primary readout, an enzyme-coupled GDP detection assay. After orthogonal and counter screens, we identified two hits with high selectivity towards MgcRacGAP, compared with other RhoGAPs, and potencies in the low micromolar range. The most promising hit, termed MINC1, was then examined with cell-based testing where it was observed to induce an increased rate of cytokinetic failure and multinucleation in addition to other cell division defects, suggesting that it may act as an MgcRacGAP inhibitor also in cells.

Keywords: Biochemical assays, cytokinesis, HTS, MgcRacGAP, Rac1, small molecule inhibitor.

INTRODUCTION

Rho GTPases are regulated molecular binary switches that cycle between active, GTP-loaded and inactive, GDP-loaded states. This protein family controls a wide array of cellular functions such as cell proliferation, apoptosis and cell morphology in health and disease [1, 2], and therefore are interesting targets for pharmacological inhibition. Small molecule modulators could have many advantages over conventional molecular biology tools such as mutant proteins and RNA interference (RNAi), which, although having provided global insight into cell biological function, seemingly led to controversial results in the Rho GTPase research field [3, 4]. Small molecule inhibitors can easily be applied in a dose-dependent, temporal or domain-specific manner, inhibiting one particular function, whereas RNAi methods completely remove the protein, disrupting possible protein-protein interactions that are mediated through domains other than the one of interest. Therefore, knockdown of proteins that have multiple functions often leads to different phenotypes observed, based on different levels of depletion. Introduction of mutant proteins might specifically target a function of interest leaving the other functions untouched; however, controlled temporal regulation is not easily achieved and non-physiological concentrations of the mutant proteins can distort the delicate balance needed for normal cellular behavior.

For the last couple of decades, protein kinases have been the most important target class in cancer drug discovery, and the majority of inhibitors achieve their activity by competing for binding with the phosphate donor substrate ATP. Like protein kinases, Rho GTPases are nucleotide-binding enzymes; therefore, it is conceivable that they could be inhibited by nucleotide-competitive small molecules. However, unlike protein kinases, which have moderate binding affinities toward ATP, Rho GTPases and most other small GTPases have very high affinity toward guanine nucleotides making them difficult to target with nucleotide-competitive small molecule inhibitors [5].

Furthermore, many of the Rho GTPases are involved in multiple cellular processes and general inhibition of a Rho GTPase may therefore have nonspecific effects. Instead, by targeting Rho protein regulators, the biological effect is expected to be more selective toward specific physiological and pathological processes. Illustrating this principle, for the 20 mammalian Rho GTPases there are more than 80 guanine nucleotide exchange factors (GEFs) that facilitate guanine nucleotide release and more than 60 GTPase activating proteins (GAPs) that stimulate the intrinsic GTPase activity [6, 7].

*Address correspondence to this author at the Institute for Molecular Medicine Finland FIMM, Nordic EMBL Partnership for Molecular Medicine, Biomedicum Helsinki 2U, P.O. Box 20 (Tukholmankatu 8), FI-00014, University of Helsinki, Finland; Tel: +358 50 415 4900;
E-mail: krister.wennerberg@fimm.fi

1875-5402/15 $58.00+.00 **© 2015 Bentham Science Publishers**

Despite the biological and therapeutic potential of small GTPase-modulating tool compounds, only a few useful compounds have been described to date, and none target a small GTPase GAP. For example, from an NIH Molecular Libraries Program screening campaign, (PubChem AID 1772) probe compounds that either antagonize or stabilize nucleotide binding in a selective or nearly selective fashion have been reported [8-12]. Specifically, one class of these modulators selectively inhibited the Rho family GTPase Cdc42 in biochemical assays and interfered with Cdc42-dependent cellular processes, such as formation of filopodia in response to bradykinin or growth factor stimulation [8, 10]. From other studies, a compound that was originally found as an inhibitor of β-amyloid processing, EHT-1864, was subsequently shown to act as an antagonist of nucleotide binding on all Rac isoforms but no other Rho GTPases [13, 14]. As a nucleotide binding inhibitor of Rac1, it blocked GEF-mediated nucleotide exchange, as well as downstream effector binding and inhibited Rac-dependent processes in cells [14]. Furthermore, a Rac1-GEF interaction inhibitor, NSC23766, was discovered by Goa and colleagues using a structure-based virtual screening approach for compounds that bind in a pocket of Rac1 that is important for GEF specific regulation [13, 15]. This compound inhibited Rac-specific GEF activity by Trio and Tiam1 in a dose-dependent manner, but not exchange activity stimulated by the promiscuous GEF Vav1, the interaction between Rac1 and the GAP BCR or the interaction between other Rho proteins, such as RhoA and Cdc42, and their GEFs. Finally, brefeldin A blocks the activity of the Arf GEF Sec7 by stabilizing the complex between Sec7 and Arf1, thereby blocking nucleotide exchange [16]. In summary, inhibitors of small GTPases themselves, GEFs and effectors have been reported, but prior to our present study no selective modulators of small GTPase GAP activity have been described.

Male germ cell Rac GTPase-activating protein (MgcRacGAP) is essential for proper regulation of cytokinesis, a highly complex cellular process that requires tight spatial and temporal control and in which Rho GTPases and their regulators and effectors are key regulatory components [17]. At the end of anaphase, MgcRacGAP, together with Mitotic Kinesin-Like Protein 1 (MKLP1) forms centralspindlin, an evolutionarily conserved hetero-tetrameric complex [18-20]. Next, the RhoGEF Ect2 localizes to the central spindle and associates with centralspindlin to form the MgcRacGAP/MKLP1/Ect2 complex that stimulates and controls RhoA, resulting in the correct localization of the contractile ring and the subsequent completion of cytokinesis [19, 21]. While this process is well-studied, the detailed functional role of MgcRacGAP, its relevant target GTPase and its GAP activity in cytokinesis have been debated and are not yet fully resolved [22-24]. The controversies and conflicting results on the role of MgcRacGAP and its GAP activity reported in the literature could very well arise from differential functions in different cell types and species [3, 25], but are also a likely outcome of studying a highly temporally controlled process by using genetic and molecular biology tools that are not temporally controlled and cannot easily be dosed.

Furthermore, MgcRacGAP appears to play essential roles in other cellular processes. First, in both cancer and development, when the MgcRacGAP/MKLP1/Ect2 complex proteins are expressed at high levels, their function has been linked to controlling polarity and driving epithelial-to-mesenchymal transition [26-30]. Second, it was described that high MgcRacGAP mRNA expression in high-risk early breast cancer as well as hepatocellular carcinoma is associated with poor disease-free survival and has a greater prognostic significance than traditional mitotic markers [31, 32]. Last, MgcRacGAP, together with Ect2, Rac1 and Cdc42, regulates centromere maintenance and stable incorporation of CENP-A after mitosis [33]. Thus, it appears that MgcRacGAP is involved in a number of physiological and pathological processes.

With the uncertainties about the role of MgcRacGAP, as well as the lack of chemical tools to probe its function, we set out to identify an MgcRacGAP inhibitor that would provide insight into the biological role of MgcRacGAP. To this end, we designed a high throughput screening strategy to identify compounds inhibiting MgcRacGAP and report here the discovery of MINC1, a selective MgcRacGAP inhibitor that interferes with MgcRacGAP function biochemically and appears to interfere with its function in cells. Since no small molecule inhibitors of MgcRacGAP or any other small GTPase GAP have been described previously, this compound and future similar chemical probes can be powerful tools for the research community to better define the complete function of MgcRacGAP. Finally, the discovery of this tool compound suggests that development of inhibitors of other small GTPase GAPs is possible.

MATERIALS AND METHODS

Protein Expression and Purification

Expression vector for MgcRacGAP GAP domain was constructed by ligating the cDNA corresponding to codons for residues 345-618 of human MgcRacGAP (NCBI accession no. NM_013277) between the EcoR I and Xho I restriction sites of pGEX-4T-1 (GE Healthcare). Expression vectors for BCR GAP domain (residues 1010-1271 of human BCR (NP_004318)), p50RhoGAP GAP domain (residues 205-439 of mouse p50RhoGAP (NP_001139374)), PAK1 PBD domain (residues 72-132 of human PAK1 (AAC50590) and Rac1 Q61L (NP_008839) were analogous to constructs that have been described previously [34, 35]. The F28L variant of human Rac1 was produced by PCR-based Phusion Site-Directed Mutagenesis (Thermo Scientific) and subcloned into the bacterial expression vector pGEX-4T-1 [35]. All DNA constructs were confirmed by DNA sequencing.

E. coli DH5α were transformed with the pGEX constructs, and recombinant proteins were purified as described by García-Mata *et al.* [36]. Protein concentrations were determined using a NanoDrop photospectrometer (Thermo Scientific) and Bradford protein assay, while protein purities were analyzed by SDS-PAGE and Coomassie Blue staining.

Biochemical GAP Activity Assays

The primary GAP assay was performed with 600 nM Rac1(F28L) in 15 mM Hepes (pH 7.5), 20 mM NaCl, 1 mM

EGTA, 0.02% Tween 20, 0.1 mg/mL bovine serum albumin, 2% DMSO and 150 μM GTP, in the presence or absence of GAP domain protein at room temperature for 2 h. GAP domain construct concentrations were titrated for use in a linear range and concentrations used were normalized to keep similar GAP activity as judged by signal window: MgcRacGAP(345-618) at 2 nM, BCR(1010-1271) at 200 nM and p50RhoGAP(205-439) at 50 nM. DMSO up to 4% had no adverse effect on assay performance. The assay was run in 96-, 384- and 1536-well format at 20, 5 and 2.5 μL volumes, respectively.

To measure the amount of GTP hydrolysis, the ADP Hunter Plus assay kit (DiscoveRx) was used according to the manufacturer's instructions at half-volumes. Resorufin fluorescence was measured at excitation at 530 nm and emission at 590 nm using a PHERAstar FS (BMG Labtech) multilabel plate reader.

Inorganic phosphate detection was performed with a malachite green assay (Biomol Green, Enzo Life Sciences) under primary assay conditions. To create a substantial light path for absorbance detection, the assay was run in 384-well half-area plate format at 15 μL volume and 15 μL of Biomol Green was added to the sample. After 30 min of incubation, the absorbance was read at 620 nm.

GTP hydrolysis by wild type Rac1 was measured using the GTPase/GAP/GEF-Glo Bioluminescent Assay System (Promega-prototype kit) as recommended by the manufacturer. Briefly, GTPase and different concentrations of MINC1 were prepared as a 2x solution containing 2 μM Rac1 and 2 μM dithiothreitol in GTPase/GAP Reaction Buffer. Next, MgcRacGAP was diluted serially into the GTPase solution (0.1-100 nM), and this solution was incubated at RT. After 2h, 2x GTP solution (10 μM) was added and the solution incubated for an additional 2h to allow the GTPase reaction. The reaction was terminated by the addition GTPase-Glo Reagent and incubation for 30 min followed by addition of Detection Solution. After 10 min, luminescence was measured using a PHERAstar FS (BMG Labtech) multilabel plate reader.

Small Molecule Compounds

The 20,480 compounds from a chemical diversity collection (ChemDiv) were transferred by the Echo 550 Liquid Handler (Labcyte) from 1 mM stock solutions into 1536-well assay plates for single dose testing (see Supplementary Table **2** for complete protocol). Compounds identified in single dose screening were subjected to dose response testing at a 0.1-100 μM concentration range against MgcRacGAP, p50RhoGAP and BCR using the primary assay conditions and readout. The 342,046 compounds from the NIH Molecular Libraries Small Molecule Repository were screened in a similar fashion (See PubChem AID 624330 for complete protocol). MINC1 (PubChem CID 744230) in the ChemDiv small molecule library (4135-0021) was reordered for confirmatory testing from Asinex (BAS 07310573) and ChemBridge (6035924) as well as resynthesized in our laboratories (Supplementary Fig. **S2**, **S3** for mass spectrometry spectra and Supplementary Table **3** for MINC1 compound usage). MINC2 was reordered from NCI/DTP (NSC72365).

Synthesis of MINC1

Reagents were obtained from Sigma–Aldrich, TCI Europe, and Merck, and solvents used were of pro analysis quality. Ethylene diamine dihydrochloride was prepared from ethylene diamine by adding 10% HCl, filtered and dried *in vacuo*. Nuclear magnetic resonance spectra data can be found in supplementary material (see Supplementary data).

n-BuOH (3.7 mL) and H_2O (19 mL) were added to dimethyl naphthalene-2,6-dicarboxylate (3.66 g, 15 mmol, 100 mol-%). Aq. NaOH (6.25 M, 4.3 mL, 210 mol-%) was added carefully, and the suspension formed was refluxed at 100 °C for 1h. After a clear solution was obtained the reaction was cooled for 10 min. The organic and aqueous phases were separated, and H_2SO_4 (0.98 mL, 17.4 mmol, 116 mol-%) was added to the aqueous phase. The resulting precipitate was filtered, washed with H_2O, and dried *in vacuo* to produce naphthalene-2,6-dicarboxylic acid (2.94 g, 91%) as a white solid.

To a suspension of naphthalene-2,6-dicarboxylic acid (865 mg, 4.0 mmol, 100 mol-%) in ethylene glycol (3 mL), ethylene diamine (0.53 mL, 8.0 mmol, 200 mol-%), ethylene diamine dihydrochloride (1.06 g, 8.0 mmol, 200 mol-%), and *p*-toluenesulfonic acid monohydrate (63 mg, 0.33 mmol, 8.3 mol-%) were added sequentially. The reaction was heated to 190 °C, forming a clear solution, which was stirred for 15 h, returning to a suspension in the end. The reaction was cooled to room temperature, and aq. HCl (20.6 mL, 267 mM) was added resulting in a clear solution to which aq. NaOH (8 mL, 12.5 M) was added. The resulting yellow precipitate was filtered, washed with H_2O and dried *in vacuo*. The hydrochloride salt was obtained by slowly adding 10% HCl solution to a suspension of the product in MeOH (8.5 mL). The precipitated final product was filtered and dried *in vacuo* to yield 2,6-bis(4,5-dihydro-1H-imidazol-2-yl)naphthalene dihydrochloride, MINC1, (428 mg, 38%) as a yellow solid.

Data Analysis

Z'-factor values were calculated for each plate, after which plates with Z'-factor values lower than 0.5 were excluded from further analysis [37]. The positive and negative control values for each plate were normalized as 100% and 0% GAP inhibition, respectively, and used to calculate a normalized activity of each compound tested. Compounds showing inhibition greater than three standard deviations (SDs) for the primary assay and more than 30% for the orthogonal assay were considered as hits. In selectivity screening, compounds showing inhibition greater than 50% for the primary assay and smaller than 15% in counter assay were considered as hits. High throughput screening (HTS) data derived from the compounds screened under NIH Molecular Libraries Program screening campaign were analyzed using ActivityBase software (IDBS, Inc). All other HTS data were processed with programs written in Matlab (R2010a, MathWorks). Four parameter dose-response curves were fit and constrained by 0% and 100% inhibition as minima and maxima, respectively using GraphPad Prism 5 (GraphPad Software). The graphs were

constrained by 0% and 100% inhibition as minima and maxima, respectively.

MgcRacGAP - Rac1 Q61L Binding Assay

Protein-protein interaction dynamics between MgcRacGAP and Rac1 (Q61L) were analyzed by bio-layer interferometry measured with an Octet Red 384 (ForteBio) using 384-well tilted-bottom plates (ForteBio, 18-5076). GST-MgcRacGAP(345-618) (100 ng/µL, in 1x PBS with 2% DMSO) was immobilized on Anti-GST Dip and Read Biosensor (ForteBio, 18-5096) for 5 min. Subsequently, the sensor was submerged for 5 min in a solution containing Rac1Q61L (50 ng/µL, in 1x PBS with 2% DMSO) and 10 min in 1x PBS with 2% DMSO to determine dissociation rates, in the presence of 12.5-50 µM MINC1 or DMSO. All steps were conducted at room temperature. The data were obtained with Octet Data Analysis Software (version 7.1.0.35, ForteBio) and curves were plotted using GraphPad Prism 5.

Cytotoxicity and Cell Proliferation Assays

HeLa (cervical epitheloid carcinoma), MDA-MB-231 (mammary gland epithelial adenocarcinoma), A549 (alveolar basal epithelial adenocarcinoma) and RWPE-1 (HPV-18 immortalized prostate) cells, obtained from ATCC, were cultured in Eagle's minimal essential medium (EMEM), Dulbecco's modified Eagle's medium (DMEM) or Roswell Park Memorial Institute (RPMI) 1640 medium, with 10% fetal bovine serum and plated in replicate sets at 1,600 cells/well in 384-well plates 6-12 h prior to drugging. Cells were exposed for up to 72 h to 5-80 µM MINC1, DMSO (negative control) or 20 µM benzethonium chloride (positive cell killing control) to identify compounds that are directly toxic to cells. CellTox Green (Promega) was added to the growth medium according to manufacturer's recommendations, and the cells were followed by live cell imaging using an IncuCyte FLR microscope (Essen Bioscience) to determine toxicity (CellTox Green fluorescence, Promega) and proliferation (phase contrast confluency). These image data were quantified with the IncuCyte application software (version 2011A rev2) and extracted cell toxicity and proliferation data were plotted with GraphPad Prism.

PAK-PBD Rac1-GTP Pull Down

MDA-MB-231 cells were transfected 24 h after plating with pBABEpuro MgcRacGAP using FuGENE HD. The next day, cells were treated with either 30 µM MINC1 or growth medium only and after 6 h incubation, the cells were lysed in 20 mM Hepes (pH 7.5), 150 mM NaCl, 1% Triton, 1 mM $MgCl_2$ and protease inhibitor cocktail set III (Millipore, 539134). Subsequently, 30 µg of GST-PAK-PBD on sepharose beads was added to the concentration-equalized lysates and incubated for 30 min at 4°C. The bead pellet was washed three times with the lysis buffer and subsequently resuspended in SDS-PAGE sample buffer. The proteins were separated on a 12% SDS-PAGE gel, transferred to a PVDF membrane and subsequently blotted for using anti-Rac1 antibody (BD Transduction Labs, 610650).

FUCCI Cell Cycle Reporter Assays

Premo FUCCI Cell Cycle Reporter (Life Technologies, P36237) was used according to manufacturer's recommendations to follow cell cycle progression and division. Briefly, cells were plated in 6-well plates at 50,000 cells/well, and 24 h later Premo gemini-GFP and Premo Cdt-RFP were added 1:1 to the cell culture medium. After overnight incubation, cells were trypsinized, subsequently plated at 1,600 cells/well and imaged every hour with phase contrast, green and red fluorescence using an IncuCyte ZOOM microscope (Essen Bioscience). 80 µM MINC1, DMSO (negative control) or 20 µM benzethonium chloride (positive for cell killing) were added 14 h later and cells were continuously followed every h.

Cell Cycle Synchronization Using a Double Thymidine Block

HeLa cells were plated in the presence of 2 mM thymidine. After 19 h, the cells were washed three times with 1x PBS before fresh culture medium was added. The second 2 mM thymidine block was applied 9 h after release. The cells were washed with 1x PBS 16 h later and released in the presence or absence of MINC1 (10-80 µM) or nocodazole (165 nM). The cells were followed by live cell imaging using an IncuCyte ZOOM microscope.

Immunofluorescence Analysis

HeLa and A549 cells were plated on fibronectin-coated coverslips or chamber slides (Nunc, 154534), respectively, at equal densities and treated for 3-48 h with either DMSO or 25 µM MINC1. Next, HeLa cells were fixed with ice-cold methanol and incubated with mouse anti-α-tubulin (Sigma Aldrich, T9026) and goat anti-MgcRacGAP (Abcam, ab2270), using goat anti-mouse Alexa Fluor 488 (Life Technologies, A11017) or donkey anti-goat Alexa Fluor 647 (Life Technologies, A-21447) to detect the primary antibodies, respectively. A549 cells were fixed and stained as described previously [38], using Alexa-555 Phalloidin (Life Technologies, A34055), Hoechst 33342 (Life Technologies, H1399) and the abovementioned antibodies. Coverslips were mounted with reagent containing DAPI when appropriate (Life Technologies, P36931 and P36930) and imaged using a Nikon 9i fluorescence microscope and NIS elements AR software (Nikon). Color balance was normalized for all images using ImageJ (NIH). The cells were scored for four different morphologies, normal (mononuclear), mitotic (rounded up), multinuclear and dead cells, using at least eight randomly chosen fields per condition.

Cellular Movement

A549 cells were plated in 96-well ImageLock plates (Essen Bioscience, cat. #4379) at 10,000 cells/well and after 6 h treated with either DMSO or 25 µM MINC1. The cells were imaged every five minutes with an IncuCyte ZOOM (Essen Bioscience) microscope using a 20x objective for a total time of 24 h. Afterwards, randomly selected cells were analyzed by Cell-IQ Analyser software (CM Technologies) to track individual cell movement.

Wound Healing

MgcRacGAP was depleted from MDA-MB-231 cells by RNAi. Specifically, cells were transfected, at a density of 350,000 cells in a single well of a 6-well plate, with siRNAs for MgcRacGAP (12.5 ng, pooled Qiagen SI00101178 and SI04954880) or a scrambled sequence control (Qiagen, 1027280) by Lipofectamine 2000. The following day, the cells were trypsinized and plated at 40,000 cells/ well in a Matrigel precoated 96-well ImageLock plate (Essen Bioscience, cat. #4379). After 16 h, the near confluent cell monolayers were scratched, washed and subsequently covered with 50 µL Matrigel (8 mg/mL, BD Bioscience 356231). After 30 min incubation at 37°C, growth medium containing either DMSO or MINC1 (final concentration 10-40 µM) was added. Normal growth medium was added to the siRNA treated cells. The plate was left in an IncuCyte microscope with the Scratch Wound assay protocol running. Using the Scratch Wound analysis software, relative wound density was determined for each image and subsequently plotted with GraphPad Prism.

RESULTS

Development of a Robust Miniaturized Screening Strategy for MgcRacGAP

As opposed to many ATP-binding proteins that have been successfully targeted in drug discovery, small GTP-binding proteins typically have very high affinity for nucleotide (micromolar versus picomolar, respectively) making them more challenging targets [5]. Specifically, since nucleotide binding is very tight, a biochemical assay with wild type small GTPases effectively becomes a near-single turnover assay, which is not practical for HTS. In the case of heterotrimeric G-proteins, Zielinski and coworkers overcame the challenge of high affinity nucleotide binding by constructing a variant of the $G\alpha_{i1}$ GTPase subunit with a mutation in the conserved TCAT loop that contacts the guanine ring. This mutant showed increased GDP dissociation, which enabled measuring multiple rounds of turnover of GTP to GDP facilitated by the RGS4 (Regulators of G-protein Signaling 4) GAP in a competitive fluorescence polarization immunoassay [39].

To study the function of MgcRacGAP in a biochemical assay we substituted the target GTPase, wild type Rac1, with a mutant Rac1 (F28L) with a lowered nucleotide affinity, typically referred to as a fast-cycling mutant [40]. With this substitution, we overcame the single turnover dynamics, creating an HTS-compatible GTPase assay dependent on GAP-mediated GTP hydrolysis (Fig. **1**). Specifically in this setup, GDP dissociated from the GTPase in the absence of a GEF, creating a continuous GTPase cycle in a GTP-rich environment, with the GTPase step as the rate-limiting factor, that enhanced sensitivity of the hydrolysis assay significantly and appeared well-suited for HTS (Fig. **1C**). The Rac1 (F28L) protein allowed for a 3-4-fold signal window between intrinsic and GAP-stimulated GTPase activities while remaining in a linear response range of GAP concentrations. Notably, MgcRacGAP did not exhibit GAP activity toward RhoA (data not shown), consistent with previous studies suggesting that MgcRacGAP is a GTPase-activating protein for Rac1 and not RhoA [3].

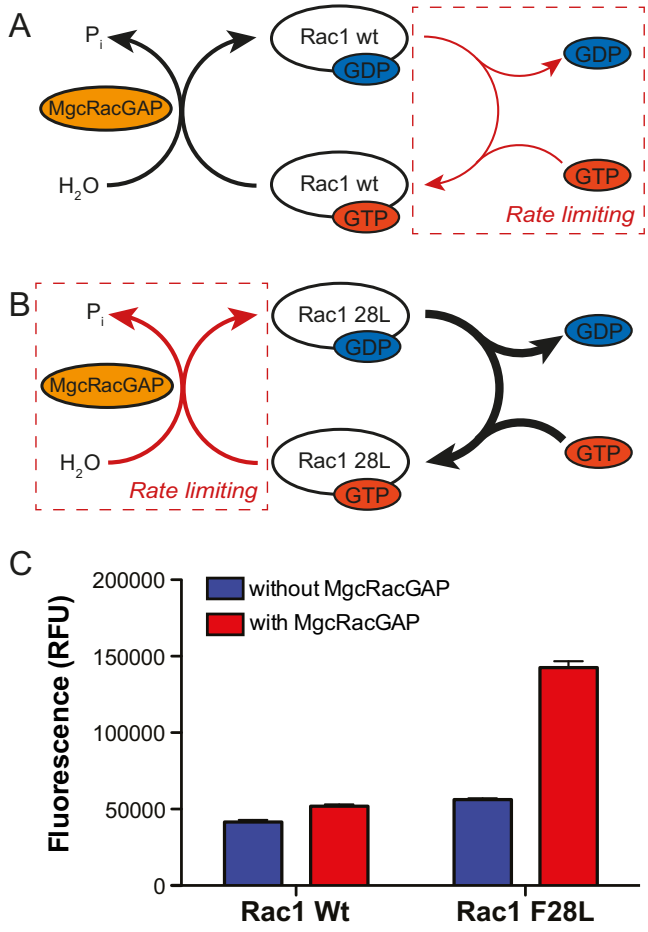

Fig. (1). Design and validation of an HTS-compatible assay measuring the biochemical activity of MgcRacGAP. **A**) Wild type Rac1 cycles between GDP- and GTP-bound forms, but owing to a very high affinity towards the guanine nucleotides, the exchange step is highly rate limiting (red arrow). **B**) Rac1(F28L) exhibits a reduced affinity for nucleotide, and therefore, a higher rate of nucleotide exchange compared to wild type Rac1. Thus, with Rac1(F28L) the GTPase step is rate limiting (red arrow) producing a sensitive, multiple turnover GAP assay. **C**) A comparison of fluorescence-mediated detection of GDP released from the GAP assay using wild type Rac1 or Rac1(F28L) shows that the fast-cycling mutant Rac1(F28L) allows for sensitive detection of GDP (GAP activity). Error bars represent SD (n=7 for each condition; $p<0.0001$, ANOVA) (color image is available online).

The GAP-stimulated Rac1 GTPase reaction could be measured effectively using both malachite green to detect production of inorganic phosphate and the ADP Hunter Plus assay kit from DiscoveRx to detect production of GDP. When the two assays were compared in terms of Z'-factor values [37], the ADP Hunter Plus assay gave higher and more consistent Z'-factors than the malachite green assay. Average Z'-factor values were 0.75 and 0.55 for the ADP Hunter Plus assay and malachite green readouts, respectively. Therefore, we chose to use the ADP Hunter Plus assay as the primary detection assay method. The malachite green assay, on the other hand, was chosen as an orthogonal validation screening strategy given that it both detects a different analyte and is based on a different detection readout (absorbance *vs* fluorescence).

After confirmation of Rac1 F28L as a fast-cycling mutant and the readout methods used, the MgcRacGAP-Rac1 assay (Fig **1**) was optimized for incubation times as well as protein and GTP concentrations in a 96-well format to make it HTS compatible. To mimic 100% inhibition of the GAP activity, MgcRacGAP was omitted from the assay mix. The biochemical assay was successfully miniaturized to 384- and 1536-well formats using automated liquid handling, showing consistent Z'-factor values ≥ 0.6 (Table **1**) and confirming that the assay was HTS-compatible.

Table 1. Optimization and validation of the HTS assay.

		96-Well		384-Well		1536-Well	
		-	+	-	+	-	+
1	CV	6.7%	6.9%	5.0%	4.8%	6.8%	4.2%
	Signal window	2.9		3.7		2.2	
	Z'-factor	0.58		0.75		0.61	
2	CV	n/a		5.5%	5.4%	5.7%	4.4%
	Signal window	n/a		3.7		3.2	
	Z'-factor	n/a		0.72		0.73	

The biochemical GAP activity assay was optimized for incubation times, protein and GTP concentrations in a 96-well format and subsequently miniaturized to 384- and 1536-well formats using automated HTS liquid handling (Z'-factor values ≥ 0.6). Negative and positive controls are referred to as - and +, respectively. The coefficient of variation (CV) is the ratio of the standard deviation to the mean whereas the signal window is the ratio of both means. The 96-well assay validation was not repeated, (indicated as n/a in the table).

High Throughput Screening Identifies Selective MgcRacGAP Inhibitors

After optimization we performed a high throughput screen using a chemical diversity set from ChemDiv at 20 μM final concentrations. Compound responses from the assay plates with Z'-factor values between 0.65 - 0.81 were analyzed (Fig. **2A**). As expected, the majority of the 20,480 compounds analyzed showed little or no GAP inhibition, (Fig. **2B**). We set the active threshold at three standard deviations over the mean, resulting in 245 active compounds (Fig. **2B**).

The hit compounds from the primary screen were retested in an orthogonal malachite green assay where 37 showed at least 30% inhibition (3.5xSD, Fig. **2C**, supplementary Table **1**) and therefore, were considered confirmed hits. To exclude the compounds that target Rac1 directly or inhibit GAPs non-selectively, the 37 compounds were examined in a counter screen using the RhoGAP domain of BCR in place of MgcRacGAP. Nine compounds showed robust selective inhibition of MgcRacGAP (>50%, vertical red line, Fig. **2D**) and weak inhibition of BCR GAP activity (<15%, horizontal red line, Fig. **2D**), when used at 10 μM. These nine compounds were then tested against the GAP domain of MgcRacGAP, BCR and p50RhoGAP in a dose response fashion, and two compounds showed high selectivity for MgcRacGAP over BCR and p50RhoGAP. When obtained from alternate sources and resynthesized, one of the two selective compounds (CID 744230, Fig. **3A**) showed reproducible, MgcRacGAP-selective dose response curves with an IC_{50} of 15±5 μM (Hill slope 0.9) and no detectable activity towards BCR and p50RhoGAP (Fig. **3C**). We named this compound MINC1 (MgcRacGAP Inhibitor Compound 1). Thus, from a screening campaign of 20,480 compounds, we identified and confirmed one compound that showed selective biochemical inhibition of MgcRacGAP.

To identify additional MgcRacGAP-inhibitory compounds, the primary assay was screened against 342,046 compounds from the NIH Molecular Libraries Small Molecule Repository chemical collection (PubChem AID 624330). Using the same active threshold of three standard deviations over the mean, we identified 4,243 compounds as active. After the primary assay, compounds determined previously as active in another Molecular Libraries Program screen (PubChem AID 1903) utilizing the ADP Hunter Plus detection system were filtered out as likely false positives. The remaining 2,362 compounds were screened with the orthogonal inorganic phosphate detection counter screen to further filter the positive hits, resulting in 557 compounds that showed >30% inhibition. Although not all Molecular Libraries Small Molecule Repository compounds could be computationally filtered, the filtering brought the orthogonal assay confirmation ratio from 15% (ChemDiv 37/245) to almost 25% (Molecular Libraries Small Molecule Repository 577/2362). Subsequently, we focused on the 117 most potent compounds (> 50% inhibition) and checked for promiscuity by examining activity in other bioassays reported in PubChem. As a result, we identified 13 compounds that tested positive in a maximum of 2.5% of the previously reported bioassays, and these compounds were chosen for testing in a dose response assay against MgcRacGAP, BCR and p50RhoGAP using the orthogonal malachite green assay. From these 13 compounds, one, MINC2 (CID 251705, Fig. **3B**) exhibited selectivity for MgcRacGAP over BCR and p50RhoGAP, and selectively was confirmed in screens with reordered compound (Fig. **3D**). In conclusion, after screening more than 360,000 compounds, we discovered two compounds of which MINC1 was the most promising hit and, therefore, used for followed-up studies.

MINC1 Acts on the Rac1-MgcRacGAP Complex

We observed that if the proteins were pre-incubated with MINC1 before GTP was added to start the GTPase reaction, the dose response curves shifted and the IC_{50} decreased almost one order of magnitude to 2±1 μM (Hill slope 0.7) while no detectable activity was seen towards BCR or

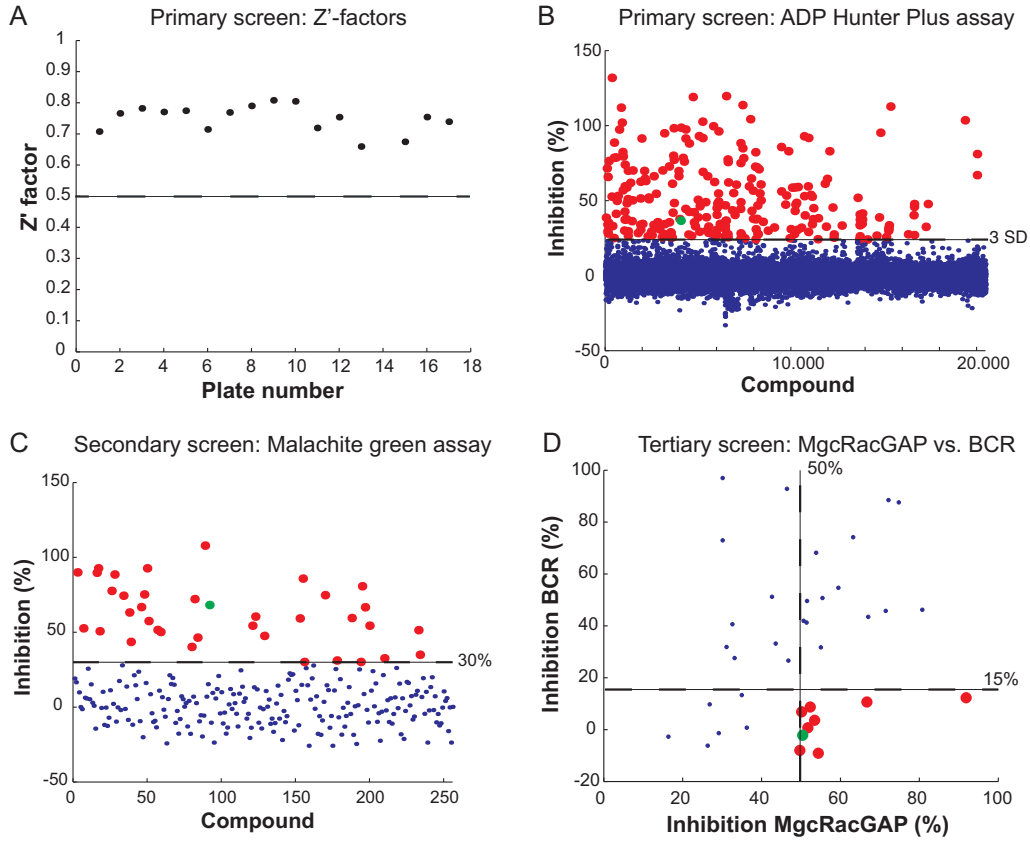

Fig. (2). Identification of an MgcRacGAP inhibitor through a novel type of screening assay. **A**) Z'-factor values from plates used in the primary screen. One plate with Z'-factor value lower than 0.5 was excluded from further analysis (#14, Z'-factor -13.55). All of the remaining plates showed Z'-factor values >0.68. **B**) A screen of 20,480 chemically diverse compounds (ChemDiv) at 20 μM. The dotted black line represents the three SDs hit cutoff. MINC1 is shown as green dot and red dots show the remaining 244 primary hit compounds. **C**) Orthogonal screening results to exclude hits resulting from inhibition of reagents of the primary assay detection system. Malachite green was used to detect GTPase turnover, and 37 compounds, shown as green (MINC1) and red dots, resulted in ≥ 30% inhibition (3.5xSD, represented by the dotted black line). **D**) Counter screen for selectivity. BCR GAP domain was used to exclude compounds that target either Rac1 or RhoGAPs in general. Of the 37 compounds testing positive through the orthogonal screen (**C**), 8 compounds, at 10 μM, shown as red dots and MINC1 as green dot, resulted in high inhibition of MgcRacGAP (>50%, vertical dotted black line) and low inhibition of BCR GAP (<15%, horizontal dotted black line) (color image is available online).

p50RhoGAP (Fig. **3E**). By changing the composition of pre-incubation mix, we determined that the shift only occurred when Rac1 was included in the pre-incubation mix (Fig. **3F**) and that the pre-incubation with MgcRacGAP had no potentiating effect. However, we observed no effects on GTP hydrolysis when MgcRacGAP was substituted with a different GAP (Supplementary Fig. **S1A**) or omitted from the reaction mix (data not shown), suggesting that although the binding to Rac1 appears to be slow and the interaction with MgcRacGAP is fast, MINC1 acts selectively on the Rac1-MgcRacGAP complex. This phenomenon was further observed when we used GTP-loaded wild type Rac1 protein. Since the single turnover assay was quick (10-20 min) and started by adding GTP-loaded Rac1, there was no effect on the MgcRacGAP GAP activity by addition of MINC1 to the reaction (Supplementary Fig. **S1B**). Moreover, in multiple-turnover assays using the wild type Rac1 protein, where nucleotide exchange therefore was the rate-limiting factor, we did not detect any notable inhibition of MgcRacGAP-stimulated activity by MINC1 (data not shown).

To further investigate the effect of MINC1 on the Rac1-MgcRacGAP complex we used a label-free interaction analysis system to characterize the protein-protein binding interactions in the presence or absence of MINC1. In these experiments, we observed that pre-treatment of the complex with MINC1 slowed down the dissociation process in a dose dependent matter (Fig. **3G**), suggesting that MINC1 stabilized the Rac1-MgcRacGAP complex and thereby inhibited a GAP-catalyzed GTPase activity.

MINC1 Treated Cells Fail to Complete Cell Division

Since MgcRacGAP is necessary to complete cytokinesis and has been shown to play an important role in centromere maintenance, an MgcRacGAP inhibitor is predicted to have a significant effect on cell growth over time [3, 22, 33]. However, the expectation is that such reduced cell growth is due to MgcRacGAP inhibition and not cytotoxicity. Thus, to discriminate between MgcRacGAP inhibition and general cell toxicity, MINC1 was examined in dose response

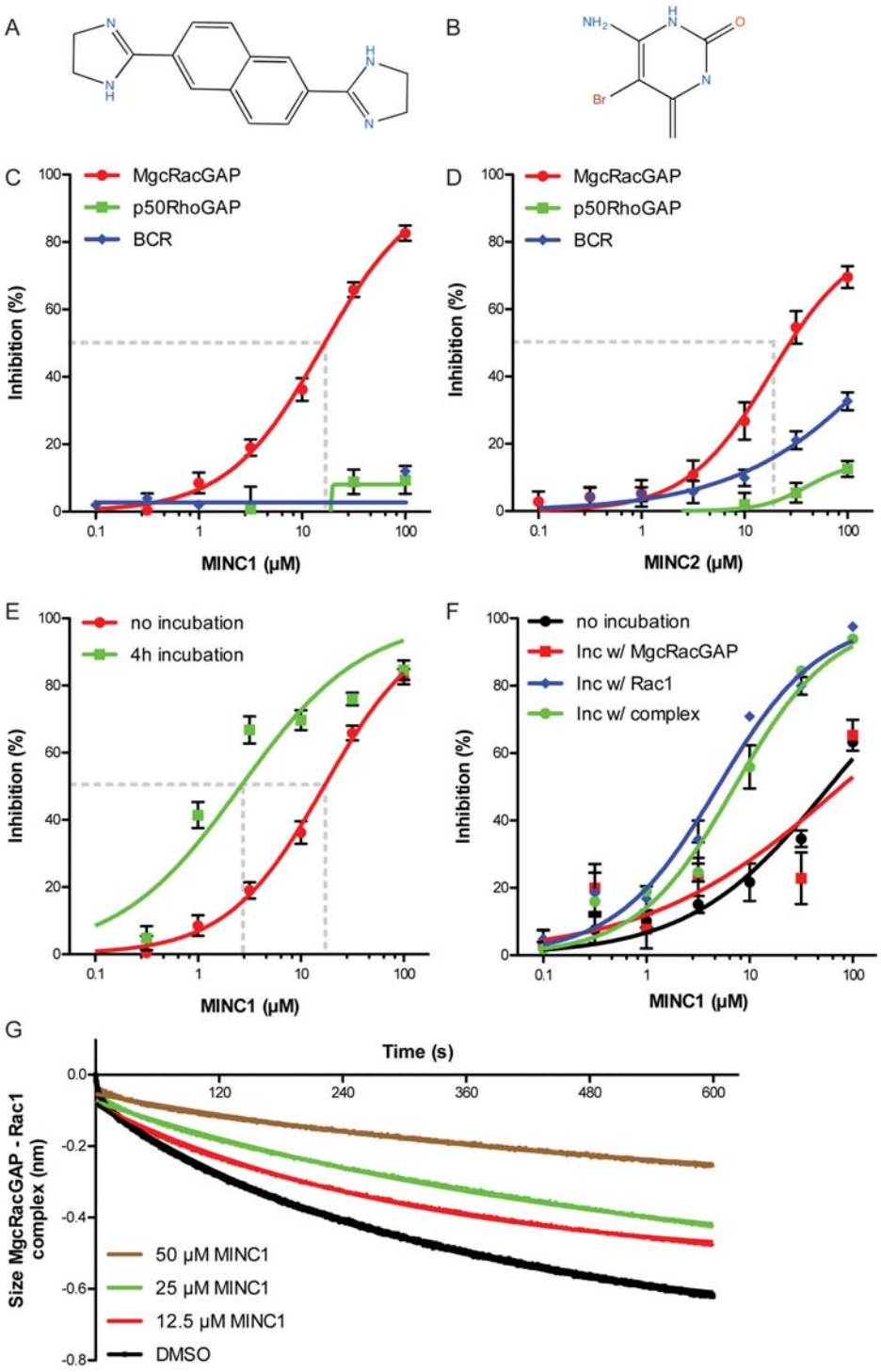

Fig. (3). Selective, **dose-dependent biochemical inhibition of MgcRacGAP by MINC1**. **A**) Molecular structure of MINC1, CID 744230. **B**) Molecular structure of MINC2, CID 251705. **C**) MINC1, identified from single dose testing, was subjected to dose response analyses (0.1-100 µM) against MgcRacGAP (red), p50RhoGAP (green) and BCR GAP (blue) in the biochemical assay. MINC1 exhibited a highly selective inhibition of MgcRacGAP, IC_{50} 15±5 µM. Error bars represent SD (n=8 for each condition). **D**) MINC2 exhibited a selective inhibition of MgcRacGAP, IC_{50} 18±7 µM. Error bars represent SD (n=3 for each condition). E) Dose response curves shift if the proteins are pre-incubated with MINC1 before GTP addition, resulting in a decreased IC_{50} by almost 1-order of magnitude. $IC_{50,\ no\ incubation}$ 15±5 µM; $IC_{50,\ incubation}$ 2±1 µM. Error bars represent SD (n=8 for each condition). **E**) MINC2 identified from single dose testing was subjected to dose response analyses (0.1-100 µM) against MgcRacGAP (red), p50RhoGAP (green) and BCR GAP (blue) in the biochemical assay. **F**) Dose response curves shift due to pre-incubation of Rac1 with MINC1. The presence of MgcRacGAP in the mixture had no additive effect on the inhibition. Error bars represent SD (n=3 for each condition). **G**) MINC1 stabilizes Rac1-MgcRacGAP complex. Pre-treatment of the complex with MINC1 slowed down the dissociation process in dose dependent matter. Error bars not presented (n=2 for each condition) (color image is available online).

analysis with various cell lines using the CellTox Green cell death assay as a toxicity readout coupled with live-cell imaging to determine cell proliferation rates. We noted that treatment with MINC1 (≥20 µM) caused cell proliferation to cease without detectable cell toxicity in highly proliferative cells (Fig. **4**) compared to negligible effects on cell viability in slow growing cells (Supplementary Fig. **S4A**, **B**). Therefore, in the subsequent experiments we used MINC1 concentrations between 20 and 30 µM to stay within the "effective window" and minimize cytotoxic side effects. Since cell death is associated with prolonged mitotic arrest [41, 42], we used live-cell imaging data to determine whether cell death occurred upon addition of MINC1 or at a later stage of the treatment. Initially, we did not observe any cell death, but as the MINC1 treatment continued and cell proliferation ceased, the percentage of cell death started to rise (Fig. **4B**, **C**, Supplementary Fig. **S4C**, **F**). Although MINC1 failed to inhibit MgcRacGAP in the wild type Rac1 biochemical assays, these results suggest that MINC1 may have the potential to inhibit MgcRacGAP in cells.

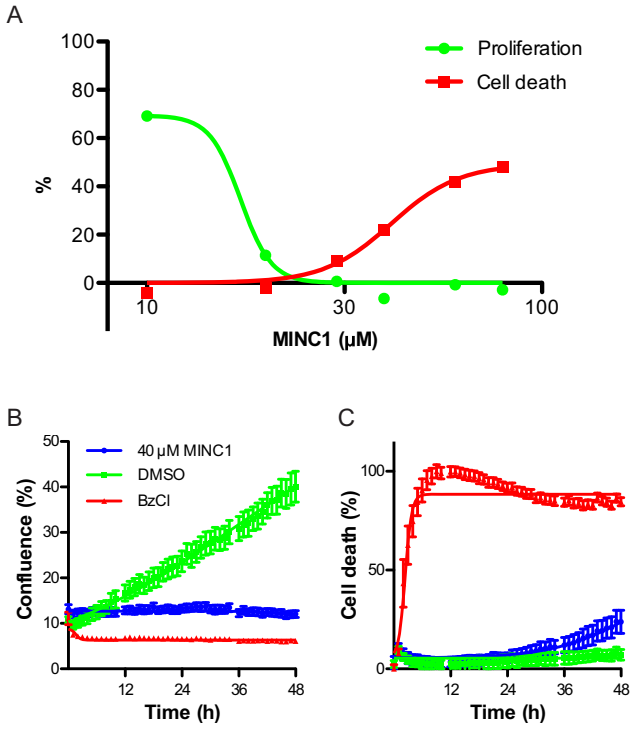

Fig. (4). Reduced rate of human tumor-derived cell proliferation without toxicity upon MINC1 treatment. **A**) MINC1 at ≥20 µM caused MDA-MB-231 cell proliferation to cease. MDA-MB-231 cells were subjected to a 48 h dose response treatment of MINC1 (5-80 µM), using DMSO and benzethonium chloride (20 µM) as negative and positive control, respectively. IC_{50} 17 µM; TC_{50} 41 µM; effective window: 2.4. **B-C**) MDA-MB-231 cells were treated with 40 µM MINC1 (blue), DMSO (green) or 20 µM benzethonium chloride (BzCl, red) and followed by live cell imaging for 48 h for proliferation (**B**, as determined by confluency) or cell toxicity (**C**). Error bars represent SEM (n=6 for each conditions) (color image available online) (color image is available online).

To examine whether MgcRacGAP activity in cells is inhibited by MINC1, we examined the GTP-loaded Rac1 levels using a PAK-PBD pull-down assay in cells [43] overexpressing MgcRacGAP in the absence or presence of MINC1. Unfortunately, overexpression of MgcRacGAP failed to detectably lower overall Rac1 GTP levels, suggesting that even when overexpressed, MgcRacGAP only acts on a small sub-pool of active Rac1 and that its activity therefore is not easily measured with a PAK-PBD pull-down assay (data not shown).

In normal division of adherent cells, cell rounding occurs upon entering mitosis, and cells spread again after the completion of mitosis [44]. When treated with MINC1, cells rounded up, but failed to complete cell division. Cell death, however, was observed only under conditions of high concentrations of MINC1 (80 µM; data not shown) for prolonged periods of time in HeLa and MDA-MB-231 cells. Interestingly, A549 cells could tolerate such high concentrations of MINC1. Therefore, we treated A549 cells with 80 µM MINC1 and followed cell cycle progression and division with the Premo FUCCI Cell Cycle Reporter to detect cells actively cycling or those arrested. Initially, very few cells displayed a fluorescence signal, but 6 h after MINC1 exposure, cells continuously fluoresced green indicating that they were arrested in G2/M-phase (Fig. **5**). To further determine whether cell rounding occurs upon entering mitosis or at any given time after the administration of MINC1, we synchronized HeLa cells using double thymidine block [45] and released them in either the presence or absence of MINC1. Unlike non-synchronized HeLa cells, where cells start to round up within approximately 3 h of MINC1 addition, MINC1-treated synchronized cells rounded up 8-10 h after release, similar to the release of nocodazole-treated cells (data not shown), indicating that the rounding occurs upon entering mitosis. These results show that the MINC1 treated cells fail to pass G2/M-phase, which is in agreement with MgcRacGAP inhibition.

To examine more deeply the effects of cell division arrest, HeLa and A549 cells were treated with 25 µM MINC1 for up to 48 h and fixed at different time points for imaging by immunofluorescence microscopy. Although plated at similar densities, MINC1-treated cells showed lower confluency in addition to multinucleation and abnormalities in cell division compared with control cells (Figs. **6**, **7**). To illustrate, a subpopulation of the MINC1-treated cells progressed into cytokinesis, but failed to complete the process, resulting in multinucleated cells (Fig. **6F**, asterisk), whereas others revealed abnormal mitotic positioning of the nuclear DNA (Figs. **6D**, **7C**, **D**, arrows). Images of MINC1-treated A549 cells taken at different time points were used to quantify for average percentage of normal, mitotic, multinucleated and dead cells (Fig. **6G**). This quantification demonstrated that the number of cells representing a mitotic phenotype peaked within the first 9 h of treatment, compared with the control cells, and the percentage of multinucleated cells increased over time during the 24h treatment. Furthermore, high-resolution images of the cells with the mitotic phenotype, revealed extensive membrane protrusions rather than the rounded phenotype seen in untreated mitotic cells, suggesting a loss of cortical actin rigidity (Fig. **7C**, **D**, arrow with round end). Thus, as predicted for an MgcRacGAP inhibitor, we observed that MINC1 treated cells showed increased

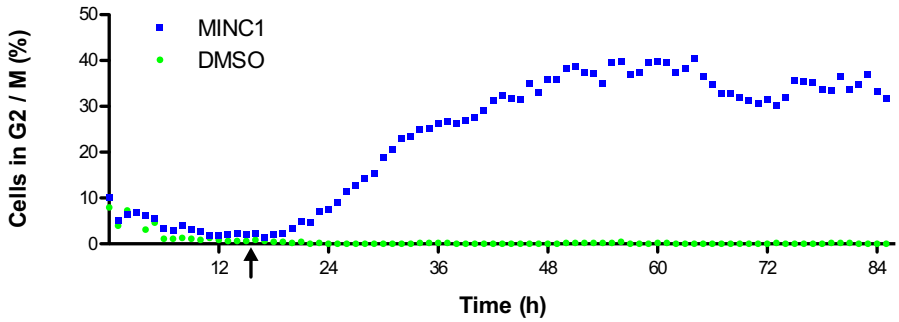

Fig. (5). MINC1-treated cells arrest in G2-/ M-phase. A549 cells transiently expressing FUCCI Cell Cycle Reporter proteins gemini-GFP (G2-/ M-phase) and Cdt-RFP (G1-/ S-phase) were treated with MINC1 (80 µM). Six hours post treatment initiation (indicated by arrow), cells started to express a green signal that did not fade, indicating that the cells were arrested in G2/M-phase. Camptothecin treatment (165 nM) was used as a positive reference.

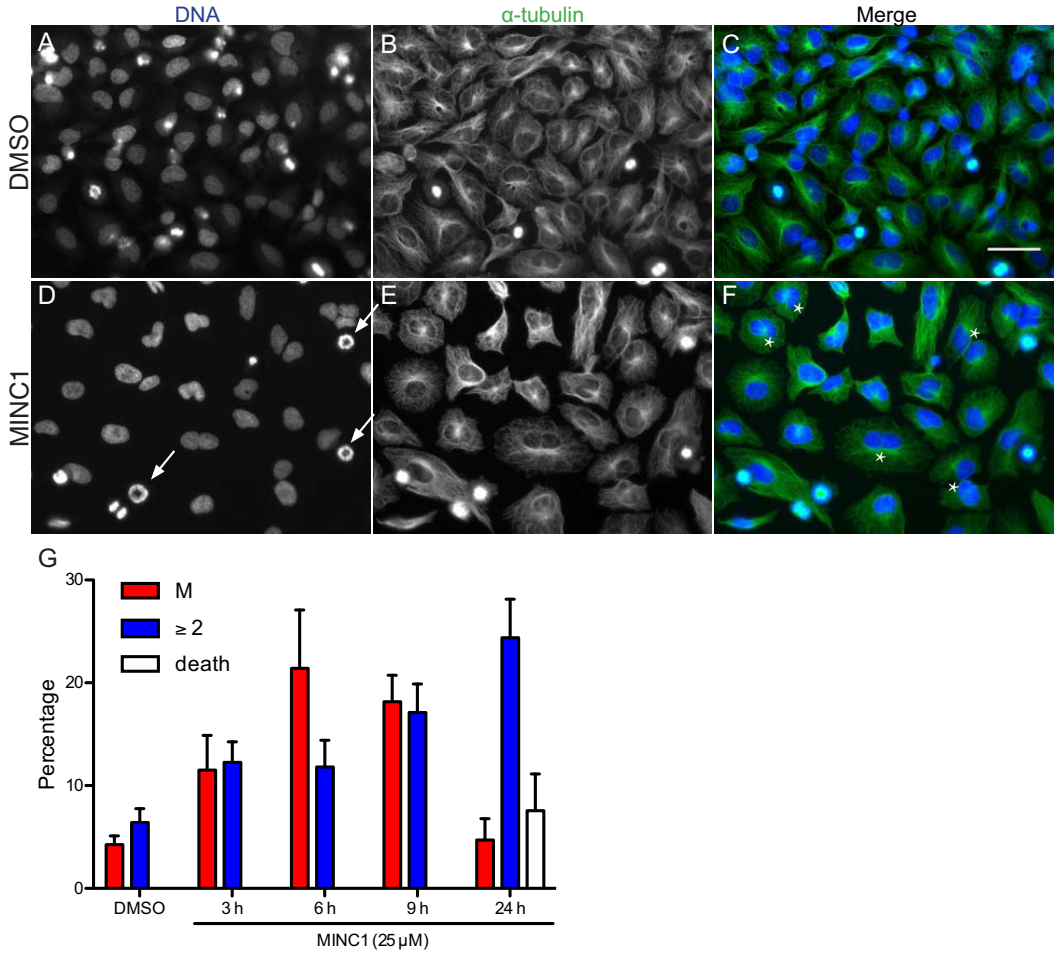

Fig. (6). Impaired cytokinesis in MINC1 treated cells. **A-F**) Representative immunofluorescence images of HeLa cells treated for 48 h with DMSO (**A-C**) or 25 µM MINC1 (**D-F**) showing DNA (left panels), α-tubulin (middle panels) and merge (right panels, DNA in blue and α-tubulin in green). MINC1 treated cells showed more multinucleated cells (asterisks panel **F**) as well as mitotic cells with collapsed spindles (arrows panel **D**) than control cells. Bar, 50 µm. **G**) Immunofluorescence images of A549 cells treated with 25 µM MINC1 were quantified for average percentage of normal, mitotic, multinucleated and death cells per time point and results are plotted as a bar graph. Error bars represent SEM (n>230 cells '24 h MINC1 treated' condition and n>320 all other conditions) (color image is available online).

numbers of multinucleated cells, but also abnormally positioned DNA.

As a result of the decreased number of rounded cells, we speculated that some cells dislodged from the culture surface, resulting in the loss of the loosely adherent population. Indeed, MINC1 treatment led to an increased population of cells that failed to attach well to the tissue culture treated plastic (data not shown). However, another

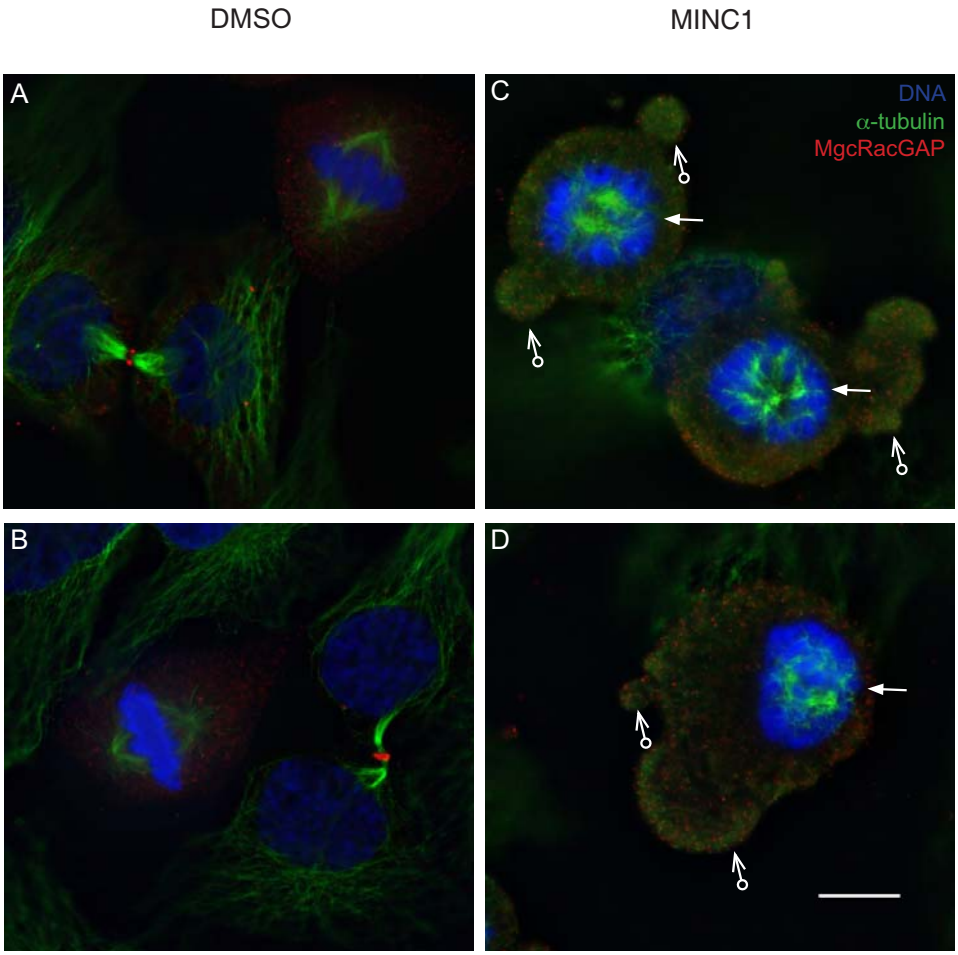

Fig. (7). Abnormal spindle morphology in the metaphase in MINC1 treated cells. Representative 60x immunofluorescence images of mitotic and cytokinetic HeLa cells treated for 48 h with DMSO (**A-B**) or 25 μM MINC1 (**C-D**) stained with antibodies to MgcRacGAP (red) and α-tubulin (green). DNA (blue) was visualized with Hoechst stain. MINC1 treated cells lacked the metaphase spindles originating from opposite poles resulting in a collapse spindle (**C-D**, indicated by arrows) and were found less frequent in cytokinetic phase compared to control cells (**A-B**). Extensive blebbing was observed in rounded-up MINC1 treatment cells (**C-D**, indicated by round ended arrows). Bar, 10 μm (color image is available online).

possibility was that the rounded cells re-adhered, which would directly explain the increased number of multinucleated cells. To determine the fate of the loosely adherent cells, we created a series of time-lapse movies in which we captured the membrane protrusions that occurred in the MINC1-treated mitotic cells (supplementary Movie S1-2). We noticed that part of the population of rounded cells indeed re-adhered to the surface, whereas others stayed round for a prolonged period of time. After approximately 20-24h, a small part of this rounded cell population underwent apoptosis. In addition, we observed that MINC1-treated cells lost almost all motility whereas the majority of DMSO-treated cells were highly motile (Fig. **8A**). To evaluate whether the MINC1-induced loss of motility on tissue culture treated plastic also extended to migration through more complex three-dimensional extracellular matrices, we performed a scratch-wound Matrigel invasion assay with MDA-MB-231 cells treated with different concentrations of MINC1. Cells treated with increasing concentrations of MINC1 displayed decreased wound-healing rates (Fig. **8B**). Likewise, cells treated with multiple siRNAs targeting MgcRacGAP showed decreased motility compared to mock-treated counterparts (Fig. **8C**). These data demonstrate that MINC1 treatment led to abnormal cortical actin activity, failed cell division and thereby an increased population of multinucleated cells as well as a loss of cell motility.

Taken together our results show that we were able to design an HTS-compatible assay that measures the activity of MgcRacGAP and utilize this assay to identify MgcRacGAP selective inhibitors. In cell-based follow-up assays, we showed that MINC1 is not cytotoxic and that treatment of cells with MINC1 reduced cell proliferation by inhibition of cell division, consistent with inhibition of MgcRacGAP. However differences between the MINC1-induced and siRNA-mediated MgcRacGAP knockdown phenotypes suggest either that GAP inhibition of MgcRacGAP has different implications than loss of the protein or that MINC1 also affects other cell division factors than MgcRacGAP in cells.

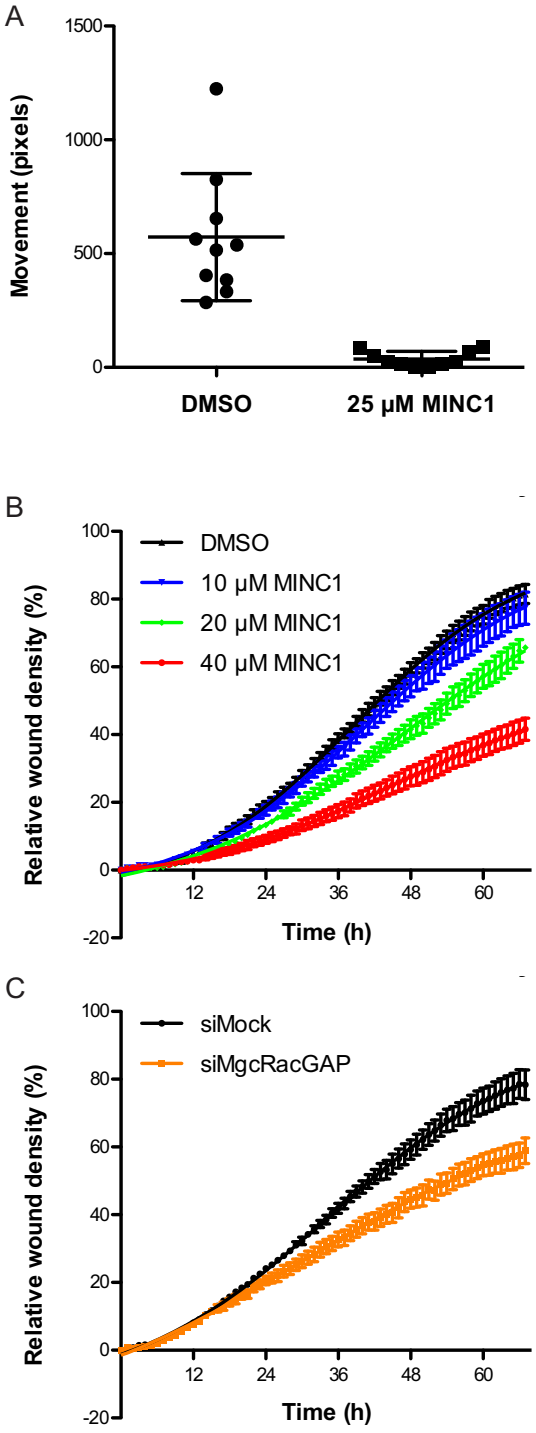

Fig. (8). Loss of cell motility in MINC1 treated cells. **A**) MINC1 treated A549 cells lose the ability to move freely in 2D culture. Cells were imaged every 5 min, and images were used to track cell movement over 24 h. **B-C**) Cells treated with increasing concentrations of MINC1 display a decreasing ability to migrate, and siRNA transfected cells show increased wound-healing times. MDA-MB-231 cells were treated with an increasing dose of MINC1 (**B**) or two pooled siRNAs targeting MgcRacGAP (**C**). Error bars represent SEM (n=4) (color image is available online).

DISCUSSION

In this study using a new HTS approach, we report the discovery of a Rho GTPase GAP inhibitor, a tool compound with selectivity for MgcRacGAP that can prove important for exploring the function of this protein in cells. Specifically, we show that this compound, MINC1, leads to a dose responsive, selective inhibition of MgcRacGAP biochemical activity as well as effects on the cellular pathways downstream of Rho family GTPase function including reduction in cell division, G2/M phase arrest, impaired cytokinesis, and reduced motility. Importantly, we believe that the MINC1 inhibitor demonstrates the success of the HTS-adapted MgcRacGAP biochemical assay and opens the door for further discovery and development of selective Rho family GAP inhibitors.

Previously, others have described high throughput format GAP assays. For example, Sun *et al.* designed a high throughput fluorescence polarization assay measuring the enzymatic activity of GTPase-activating proteins of ADP-ribosylation factors, and Zielinski *et al.* developed an assay for the GAP activity of RGS4 towards the heterotrimeric G-protein $G\alpha_{i1}$ subunit [39, 46]. While both of these GAP studies reported that small screens had been performed, no hits for the GAP proteins were described. In our study, we screened over 360,000 compounds and identified two compounds that inhibited MgcRacGAP with high selectivity over BCR or p50RhoGAP in biochemical GAP assays. The most potent of these hits, a compound we termed MINC1, inhibited cell proliferation and impaired cytokinesis, suggesting that the inhibitor is active towards MgcRacGAP in cells. Based on our results, we conclude that small GTPase GAPs are highly challenging but putatively druggable targets.

In studying the mechanism of action of the MINC1 inhibitor, we determined that while it is selective for MgcRacGAP-mediated GTP hydrolysis by Rac1, it appears to affect the GTPase-GAP complex with a slow binding to Rac1. Furthermore, we noted that complete inhibition of enzymatic activity could not be obtained with MINC1 and that dose response curves instead reached a maximum at 80-90% inhibition. Together, these data may suggest that MINC1 does not necessarily block the GAP activity of MgcRacGAP, but rather stabilizes the Rac1-MgcRacGAP complex and, by slowing down the turnover, inhibits MgcRacGAP activity, similar to what has been described for the Arf GEF inhibitor brefeldin A [16]. In support of this idea, we detected a decreased dissociation rate of the Rac1-MgcRacGAP complex in the presence of MINC1. This complex mechanism of action might also explain why we failed to detect inhibition of MgcRacGAP-mediated GTP hydrolysis in single turnover GTPase assays using wild type Rac1.

MINC1 is represented in PubChem as compound ID 744230, and it has been included in 23 reported bioassays. The only reported bioactivity is a marginal activity, at 80 µM, against the essential replicative helicase of *Staphylococcus aureus* (AID 485395). No close structural analogs of MINC1 were present in our compound collection

or commercially available; therefore, we have not explored the structure activity relationship of MINC1 with MgcRacGAP in this study.

MgcRacGAP, as well as many other small GTPase GAPs, is a key component of highly dynamic and spatially and temporally controlled cellular processes. In the past, studies of the cellular functions of MgcRacGAP have been limited to methods using RNAi or overexpression of GAP-activity-defective and other functional mutants of the protein [20, 47, 48]. Neither of these methods can be easily applied to a dose or temporal dependency and have a drawback of resulting in non-physiological concentrations, artificially high or low, of the protein in cells. Controversies in the literature regarding a specific role and function of MgcRacGAP in cytokinesis as well as other processes [3, 4] might be explained by the challenging interpretation of results of knockdown and overexpression studies. Therefore, we expected that the development of potent and selective small molecule inhibitors of MgcRacGAP would be critical for defining the detailed function and role of this protein.

An interesting example case is that of Polo-like kinase 1 (PLK1). PLK1 is an essential serine/threonine kinase that has multiple important functions in early mitotic processes, including the direct regulation of MgcRacGAP [49, 50]. Removal of PLK1 by RNAi leads to a cell-cycle arrest in the metaphase/anaphase transition with resulting monopolar spindle cells [51-53], but controversial results, which could be caused by incomplete PLK1 depletion, were obtained. The development of potent and selective PLK1 inhibitors permitted examination of the role of partial versus complete inhibition [54, 55]. Furthermore, the possibility to temporally control the inhibition allowed for detailed analysis of PLK1 in different phases of the cell cycle, demonstrating that inhibition of PLK1 induced a loss of interaction between Ect2 and MgcRacGAP in anaphase, preventing localization of Ect2 to the central spindle during late mitosis and thereby preventing initiation of cytokinesis [56].

Our studies with MINC1 revealed both expected and unexpected effects on cell division. As expected, we saw an accumulation of multinucleated cells; however, we also observed a phenotype that resembled a failure of prophase/pro-metaphase (Figs. **6**, **7**), with the chromosomes unevenly spaced from the spindle pole, similar to a PLK1-inhibited phenotype [57]. Moreover, the MgcRacGAP distribution in these prophase/pro-metaphase cells seemed to follow the α-tubulin staining, which concurs with findings of Hirose *et al.* that MgcRacGAP co-localizes with the microtubules [48]. It has been shown that inhibition of MgcRacGAP is important for the correct formation of the mitotic spindle during the metaphase. Specifically, overexpression of an MgcRacGAP mutant, whose GAP activity could not be inhibited, resulted in a lack of normal bipolar spindles [58]. Taken together with our observation of MINC1-mediated inhibition of MgcRacGAP, the results may suggest that the GAP activity of MgcRacGAP plays an important role in mitosis and that this function may be regulated by PLK1. Alternatively, our results may result from additional, yet unknown, MINC1-induced effects on the cell division machinery through other targets.

In addition to the role of MgcRacGAP in cytokinesis, several studies have shown that it plays a role in cellular polarity and migration. For example, Jacquemet and colleagues have shown that MgcRacGAP can locally suppress the activity of Rac1, resulting in upregulation of RhoA activity, thereby promoting invasive migration and that removal of MgcRacGAP by RNAi leads to the loss of invasive migration [30]. In our experiments, we demonstrated that MINC1-treated cells lost their invasive migratory properties in a dose dependent matter (Fig. **8**). Furthermore, MINC1 treatment induced extensive blebbing in mitotic cells (Fig. **7C**, **D**), in agreement with a high Rac1/low RhoA activity and loss of cortical actin rigidity resulting from blocking MgcRacGAP activity. These observations further support the idea that MINC1 affects the MgcRacGAP-Rac1 complex in cells.

In conclusion, we identified MINC1 as a putative MgcRacGAP inhibitor from a small molecule screen of over 360,000 compounds in a biochemical assay adapted for HTS. Future studies aim to use this chemical scaffold to identify compounds with higher affinity and faster binding kinetics, as well as exploring inhibitors with selectivity towards other GAPs and potential targets. Thus, although RhoGAPs are challenging small molecule targets, our study shows that they are screenable and appear druggable, and we expect that optimized analogs of MINC1 will allow us to improve the understanding of the function of MgcRacGAP in cells and investigate its role in both physiological processes and human malignancy.

AUTHOR CONTRIBUTIONS

AA performed laboratory studies, analyzed the data, and wrote the manuscript. AF, LT, AL and JS performed laboratory studies. AK coordinated the chemical synthesis. GR performed laboratory studies and wrote the manuscript. KW coordinated the project, analyzed the data, and wrote the manuscript.

ABBREVIATIONS

DMSO	=	Dimethyl sulfoxide
GAP	=	GTPase-activating protein
GDP	=	Guanosine diphosphate
GEF	=	Guanine nucleotide exchange factor
GST	=	Glutatione S-transferase
GTP	=	Guanosine triphosphate
HTS	=	High throughput screening
IPTG	=	Isopropyl β-D-1-thiogalactopyranoside
MgcRacGAP	=	Male germ cell Rac GTPase-activating protein
MINC1	=	MgcRacGAP inhibitor compound 1
MKLP1	=	Mitotic kinesin-like protein 1
PLK1	=	Polo-like kinase 1
PMSF	=	Phenylmethylsulfonyl fluoride
RNAi	=	RNA interference
SD	=	Standard deviation

CONFLICT OF INTEREST

The authors confirm that this article content has no conflict of interest.

ACKNOWLEDGEMENTS

This work was financially supported by the Jane and Aatos Erkko Foundation and a NIH Molecular Libraries Program grant (1 R03 DA033983) (KW) and by the Helsinki Biomedical Graduate Program (AA). We thank the FIMM Technology Center High Throughput Biomedicine unit and Marja Hagström from Centre for Drug Research and Division of pharmaceutical biosciences, both part of the Biocenter Finland Drug Discovery and Chemical Biology infrastructure platform for their technical support and the use of their instrumentation. We also acknowledge the technical expertise, support and use of instruments of the HTS center at Southern Research Institute. We thank Subhanjan Mondal and Said Goueli at Promega for the early access of the GTPase/GAP/GEF-Glo Bioluminescent Assay System.

SUPPLEMENTARY MATERIAL

Supplementary material is available on the publisher's web site along with the published article.

REFERENCES

[1] Hall, A. Rho family GTPases. *Biochem. Soc. Trans.,* **2012**, *40* (6), 1378-1382.

[2] Wennerberg, K.; Der, C. J. Rho-family GTPases: it's not only Rac and Rho (and I like it). *J. Cell Sci.,* **2004**, *117* (Pt 8), 1301-1312.

[3] Bastos, R. N.; Penate, X.; Bates, M.; Hammond, D.; Barr, F. A. CYK4 inhibits Rac1-dependent PAK1 and ARHGEF7 effector pathways during cytokinesis. *J. Cell Biol.,* **2012**, *198* (5), 865-880.

[4] Loria, A.; Longhini, K. M.; Glotzer, M. The RhoGAP domain of CYK-4 has an essential role in RhoA activation. *Curr. Biol.,* **2012**, *22* (3), 213-219.

[5] Sprang, S. R. G protein mechanisms: insights from structural analysis. *Annu. Rev. Biochem.,* **1997**, *66*, 639-678.

[6] Vigil, D.; Cherfils, J.; Rossman, K. L.; Der, C. J. Ras superfamily GEFs and GAPs: validated and tractable targets for cancer therapy? *Nat. Rev. Cancer,* **2010**, *10* (12), 842-857.

[7] Cherfils, J.; Zeghouf, M. Regulation of small GTPases by GEFs, GAPs, and GDIs. *Physiol. Rev.,* **2013**, *93* (1), 269-309.

[8] Surviladze, Z.; Waller, A.; Wu, Y.; Romero, E.; Edwards, B. S.; Wandinger-Ness, A.; Sklar, L. A. Identification of a small GTPase inhibitor using a high-throughput flow cytometry bead-based multiplex assay. *J. Biomol. Screen.,* **2010**, *15* (1), 10-20.

[9] Surviladze, Z.; Ursu, O.; Miscioscia, F.; Curpan, R.; Halip, L.; Bologa, C.; Oprea, T.; Waller, A.; Strouse, J.; Salas, V.; Wu, Y.; Edwards, B.; Wandinger-Ness, A.; Sklar, L. Three small molecule pan activator families of Ras-related GTPases. In *Probe Reports from the NIH Molecular Libraries Program*, Bethesda (MD), 2010.

[10] Surviladze, Z.; Waller, A.; Strouse, J. J.; Bologa, C.; Ursu, O.; Salas, V.; Parkinson, J. F.; Phillips, G. K.; Romero, E.; Wandinger-Ness, A.; Sklar, L. A.; Schroeder, C.; Simpson, D.; Noth, J.; Wang, J.; Golden, J.; Aube, J. A Potent and Selective Inhibitor of Cdc42 GTPase. In *Probe Reports from the NIH Molecular Libraries Program*, Bethesda (MD), 2010.

[11] Agola, J. O.; Hong, L.; Surviladze, Z.; Ursu, O.; Waller, A.; Strouse, J. J.; Simpson, D. S.; Schroeder, C. E.; Oprea, T. I.; Golden, J. E.; Aube, J.; Buranda, T.; Sklar, L. A.; Wandinger-Ness, A. A competitive nucleotide binding inhibitor: *in vitro* characterization of Rab7 GTPase inhibition. *ACS Chem. Biol.,* **2012**, *7* (6), 1095-1108.

[12] Hong, L.; Simons, P.; Waller, A.; Strouse, J.; Surviladze, Z.; Ursu, O.; Bologa, C.; Gouveia, K.; Agola, J. O.; BasuRay, S.; Wandinger-Ness, A.; Sklar, L.; Simpson, D. S.; Schroeder, C. E.; Golden, J. E.; Aube, J. A small molecule pan-inhibitor of Ras-superfamily GTPases with high efficacy towards Rab7. In *Probe Reports from the NIH Molecular Libraries Program*, Bethesda (MD), 2010.

[13] Desire, L.; Bourdin, J.; Loiseau, N.; Peillon, H.; Picard, V.; De Oliveira, C.; Bachelot, F.; Leblond, B.; Taverne, T.; Beausoleil, E.; Lacombe, S.; Drouin, D.; Schweighoffer, F. RAC1 inhibition targets amyloid precursor protein processing by gamma-secretase and decreases Abeta production *in vitro* and *in vivo*. *J. Biol. Chem.,* **2005**, *280* (45), 37516-37525.

[14] Shutes, A.; Onesto, C.; Picard, V.; Leblond, B.; Schweighoffer, F.; Der, C. J. Specificity and mechanism of action of EHT 1864, a novel small molecule inhibitor of Rac family small GTPases. *J. Biol. Chem.,* **2007**, *282* (49), 35666-35678.

[15] Gao, Y.; Dickerson, J. B.; Guo, F.; Zheng, J.; Zheng, Y. Rational design and characterization of a Rac GTPase-specific small molecule inhibitor. *Proc. Natl. Acad. Sci. U S A,* **2004**, *101* (20), 7618-7623.

[16] Zeghouf, M.; Guibert, B.; Zeeh, J. C.; Cherfils, J. Arf, Sec7 and Brefeldin A: a model towards the therapeutic inhibition of guanine nucleotide-exchange factors. *Biochem. Soc. Trans,* **2005**, *33* (Pt 6), 1265-1268.

[17] Piekny, A.; Werner, M.; Glotzer, M. Cytokinesis: welcome to the Rho zone. *Trends Cell Biol.,* **2005**, *15* (12), 651-658.

[18] Toure, A.; Dorseuil, O.; Morin, L.; Timmons, P.; Jegou, B.; Reibel, L.; Gacon, G. MgcRacGAP, a new human GTPase-activating protein for Rac and Cdc42 similar to Drosophila rotundRacGAP gene product, is expressed in male germ cells. *J. Biol. Chem.,* **1998**, *273* (11), 6019-6023.

[19] Mishima, M.; Kaitna, S.; Glotzer, M. Central spindle assembly and cytokinesis require a kinesin-like protein/RhoGAP complex with microtubule bundling activity. *Dev. Cell,* **2002**, *2* (1), 41-54.

[20] Jantsch-Plunger, V.; Gonczy, P.; Romano, A.; Schnabel, H.; Hamill, D.; Schnabel, R.; Hyman, A. A.; Glotzer, M. CYK-4: A Rho family gtpase activating protein (GAP) required for central spindle formation and cytokinesis. *J. Cell Biol.,* **2000**, *149* (7), 1391-1404.

[21] Yuce, O.; Piekny, A.; Glotzer, M. An ECT2-centralspindlin complex regulates the localization and function of RhoA. *J. Cell Biol.,* **2005**, *170* (4), 571-582.

[22] Canman, J. C.; Lewellyn, L.; Laband, K.; Smerdon, S. J.; Desai, A.; Bowerman, B.; Oegema, K. Inhibition of Rac by the GAP activity of centralspindlin is essential for cytokinesis. *Science,* **2008**, *322* (5907), 1543-1546.

[23] Miller, A. L.; Bement, W. M. Regulation of cytokinesis by Rho GTPase flux. *Nat. Cell Biol.,* **2009**, *11* (1), 71-77.

[24] Yamada, T.; Hikida, M.; Kurosaki, T. Regulation of cytokinesis by mgcRacGAP in B lymphocytes is independent of GAP activity. *Exp. Cell Res.,* **2006**, *312* (18), 3517-3525.

[25] White, E. A.; Glotzer, M. Centralspindlin: at the heart of cytokinesis. *Cytoskeleton (Hoboken),* **2012**, *69* (11), 882-892.

[26] Portereiko, M. F.; Saam, J.; Mango, S. E. ZEN-4/MKLP1 is required to polarize the foregut epithelium. *Curr. Biol.,* **2004**, *14* (11), 932-941.

[27] Smallhorn, M.; Murray, M. J.; Saint, R. The epithelial-mesenchymal transition of the Drosophila mesoderm requires the Rho GTP exchange factor Pebble. *Development,* **2004**, *131* (11), 2641-2651.

[28] Justilien, V.; Fields, A. P. Ect2 links the PKCiota-Par6alpha complex to Rac1 activation and cellular transformation. *Oncogene,* **2009**, *28* (41), 3597-3607.

[29] Justilien, V.; Jameison, L.; Der, C. J.; Rossman, K. L.; Fields, A. P. Oncogenic activity of Ect2 is regulated through protein kinase C iota-mediated phosphorylation. *J. Biol. Chem.,* **2011**, *286* (10), 8149-8157.

[30] Jacquemet, G.; Green, D. M.; Bridgewater, R. E.; von Kriegsheim, A.; Humphries, M. J.; Norman, J. C.; Caswell, P. T. RCP-driven alpha5beta1 recycling suppresses Rac and promotes RhoA activity *via* the RacGAP1-IQGAP1 complex. *J. Cell Biol.,* **2013**, *202* (6), 917-935.

[31] Jung, Y.; Lee, S.; Choi, H. S.; Kim, S. N.; Lee, E.; Shin, Y.; Seo, J.; Kim, B.; Jung, Y.; Kim, W. K.; Chun, H. K.; Lee, W. Y.; Kim, J. Clinical validation of colorectal cancer biomarkers identified from bioinformatics analysis of public expression data. *Clin. Cancer Res.,* **2011**, *17* (4), 700-709.

[32] Pliarchopoulou, K.; Kalogeras, K. T.; Kronenwett, R.; Wirtz, R. M.; Eleftheraki, A. G.; Batistatou, A.; Bobos, M.; Soupos, N.; Polychronidou, G.; Gogas, H.; Samantas, E.; Christodoulou, C.; Makatsoris, T.; Pavlidis, N.; Pectasides, D.; Fountzilas, G. Prognostic significance of RACGAP1 mRNA expression in high-risk early breast cancer: a study in primary tumors of breast cancer patients participating in a randomized Hellenic Cooperative Oncology Group trial. *Cancer Chemother. Pharmacol.,* **2013**, *71* (1), 245-255.

[33] Lagana, A.; Dorn, J. F.; De Rop, V.; Ladouceur, A. M.; Maddox, A. S.; Maddox, P. S. A small GTPase molecular switch regulates epigenetic centromere maintenance by stabilizing newly incorporated CENP-A. *Nat. Cell Biol.,* **2010**, *12* (12), 1186-1193.

[34] Zhang, B.; Chernoff, J.; Zheng, Y., Interaction of Rac1 with GTPase-activating proteins and putative effectors. A comparison with Cdc42 and RhoA. *J. Biol. Chem.,* **1998**, *273* (15), 8776-8782.

[35] Wennerberg, K.; Ellerbroek, S. M.; Liu, R. Y.; Karnoub, A. E.; Burridge, K.; Der, C. J. RhoG signals in parallel with Rac1 and Cdc42. *J. Biol. Chem.,* **2002**, *277* (49), 47810-47817.

[36] Garcia-Mata, R.; Wennerberg, K.; Arthur, W. T.; Noren, N. K.; Ellerbroek, S. M.; Burridge, K. Analysis of activated GAPs and GEFs in cell lysates. *Methods Enzymol.,* **2006**, *406*, 425-437.

[37] Zhang, J. H.; Chung, T. D.; Oldenburg, K. R. A Simple Statistical Parameter for Use in Evaluation and Validation of High Throughput Screening Assays. *J. Biomol. Screen.,* **1999**, *4* (2), 67-73.

[38] Canman, J. C.; Hoffman, D. B.; Salmon, E. D. The role of pre- and post-anaphase microtubules in the cytokinesis phase of the cell cycle. *Curr. Biol.,* **2000**, *10* (10), 611-614.

[39] Zielinski, T.; Kimple, A. J.; Hutsell, S. Q.; Koeff, M. D.; Siderovski, D. P.; Lowery, R. G. Two Galpha(i1) rate-modifying mutations act in concert to allow receptor-independent, steady-state measurements of RGS protein activity. *J. Biomol. Screen.,* **2009**, *14* (10), 1195-1206.

[40] Lin, R.; Cerione, R. A.; Manor, D. Specific contributions of the small GTPases Rho, Rac, and Cdc42 to Dbl transformation. *J. Biol. Chem.,* **1999**, *274* (33), 23633-23641.

[41] Sorger, P. K.; Dobles, M.; Tournebize, R.; Hyman, A. A. Coupling cell division and cell death to microtubule dynamics. *Curr. Opin. Cell Biol.,* **1997**, *9* (6), 807-814.

[42] Mollinedo, F.; Gajate, C. Microtubules, microtubule-interfering agents and apoptosis. *Apoptosis,* **2003**, *8* (5), 413-450.

[43] Benard, V.; Bohl, B. P.; Bokoch, G. M. Characterization of rac and cdc42 activation in chemoattractant-stimulated human neutrophils using a novel assay for active GTPases. *J. Biol. Chem.,* **1999**, *274* (19), 13198-13204.

[44] Thery, M.; Bornens, M. Get round and stiff for mitosis. *HFSP J.,* **2008**, *2* (2), 65-71.

[45] Bootsma, D.; Budke, L.; Vos, O. Studies on synchronous division of tissue culture cells initiated by excess thymidine. *Exp. Cell Res.,* **1964**, *33*, 301-309.

[46] Sun, W.; Vanhooke, J. L.; Sondek, J.; Zhang, Q. High-throughput fluorescence polarization assay for the enzymatic activity of GTPase-activating protein of ADP-ribosylation factor (ARFGAP). *J. Biomol. Screen.,* **2011**, *16* (7), 717-723.

[47] Kawashima, T.; Hirose, K.; Satoh, T.; Kaneko, A.; Ikeda, Y.; Kaziro, Y.; Nosaka, T.; Kitamura, T. MgcRacGAP is involved in the control of growth and differentiation of hematopoietic cells. *Blood,* **2000**, *96* (6), 2116-2124.

[48] Hirose, K.; Kawashima, T.; Iwamoto, I.; Nosaka, T.; Kitamura, T. MgcRacGAP is involved in cytokinesis through associating with mitotic spindle and midbody. *J. Biol. Chem.,* **2001**, *276* (8), 5821-5828.

[49] Wolfe, B. A.; Takaki, T.; Petronczki, M.; Glotzer, M. Polo-like kinase 1 directs assembly of the HsCyk-4 RhoGAP/Ect2 RhoGEF complex to initiate cleavage furrow formation. *PLoS Biol.,* **2009**, *7* (5), e1000110.

[50] Burkard, M. E.; Maciejowski, J.; Rodriguez-Bravo, V.; Repka, M.; Lowery, D. M.; Clauser, K. R.; Zhang, C.; Shokat, K. M.; Carr, S. A.; Yaffe, M. B.; Jallepalli, P. V. Plk1 self-organization and priming phosphorylation of HsCYK-4 at the spindle midzone regulate the onset of division in human cells. *PLoS Biol.,* **2009**, *7* (5), e1000111.

[51] Barr, F. A.; Sillje, H. H.; Nigg, E. A. Polo-like kinases and the orchestration of cell division. *Nat. Rev. Mol. Cell Biol.,* **2004**, *5* (6), 429-440.

[52] van Vugt, M. A.; van de Weerdt, B. C.; Vader, G.; Janssen, H.; Calafat, J.; Klompmaker, R.; Wolthuis, R. M.; Medema, R. H. Polo-like kinase-1 is required for bipolar spindle formation but is dispensable for anaphase promoting complex/Cdc20 activation and initiation of cytokinesis. *J. Biol. Chem.,* **2004**, *279* (35), 36841-36854.

[53] Sumara, I.; Gimenez-Abian, J. F.; Gerlich, D.; Hirota, T.; Kraft, C.; de la Torre, C.; Ellenberg, J.; Peters, J. M. Roles of polo-like kinase 1 in the assembly of functional mitotic spindles. *Curr. Biol.,* **2004**, *14* (19), 1712-1722.

[54] Steegmaier, M.; Hoffmann, M.; Baum, A.; Lenart, P.; Petronczki, M.; Krssak, M.; Gurtler, U.; Garin-Chesa, P.; Lieb, S.; Quant, J.; Grauert, M.; Adolf, G. R.; Kraut, N.; Peters, J. M.; Rettig, W. J. BI 2536, a potent and selective inhibitor of polo-like kinase 1, inhibits tumor growth *in vivo*. *Curr. Biol.,* **2007**, *17* (4), 316-322.

[55] Lenart, P.; Petronczki, M.; Steegmaier, M.; Di Fiore, B.; Lipp, J. J.; Hoffmann, M.; Rettig, W. J.; Kraut, N.; Peters, J. M. The small-molecule inhibitor BI 2536 reveals novel insights into mitotic roles of polo-like kinase 1. *Curr. Biol.,* **2007**, *17* (4), 304-315.

[56] Petronczki, M.; Glotzer, M.; Kraut, N.; Peters, J. M. Polo-like kinase 1 triggers the initiation of cytokinesis in human cells by promoting recruitment of the RhoGEF Ect2 to the central spindle. *Dev. Cell,* **2007**, *12* (5), 713-725.

[57] Tillement, V.; Remy, M. H.; Raynaud-Messina, B.; Mazzolini, L.; Haren, L.; Merdes, A. Spindle assembly defects leading to the formation of a monopolar mitotic apparatus. *Biol. Cell,* **2009**, *101* (1), 1-11.

[58] Ban, R.; Irino, Y.; Fukami, K.; Tanaka, H. Human mitotic spindle-associated protein PRC1 inhibits MgcRacGAP activity toward Cdc42 during the metaphase. *J. Biol. Chem.,* **2004**, *279* (16), 16394-16402.

Received: June 27, 2014 **Revised: November 12, 2014** **Accepted: December 3, 2014**